Available online at www.sciencedirect.com
SCIENCE DIRECT®
Journal of Sound and Vibration 271 (2004) 507–518
JOURNAL OF SOUND AND VIBRATION
www.elsevier.com/locate/jsvi

Vibration analysis of cracked rotor sliding bearing system with rotor–stator rubbing by harmonic wavelet transform

Fangyi Wan*, Qingyu Xu, Songtao Li

The State Key Laboratory of Mechanical Structure Strength and Vibration, Xi'an Jiaotong University, Xi'an Ning West Road 28, Xi'an, Shaanxi Province, 710049 China

Received 25 June 2002; accepted 10 March 2003

Abstract

In this paper, the vibration of a cracked rotor sliding bearing system with rotor–stator rubbing is investigated using harmonic wavelet transform (HWT). Three non-linear factors, non-linear oil film forces, rotor–stator rubbing and the presence of crack, are taken into account. So the non-linear behavior of the rotor will be much more complex. According to Newmark method, the dynamic response of the rotor is calculated. Using HWT method, the effect of these non-linear factors is analyzed simultaneously in both time and frequency domain. The numerical simulated result shows that HWT will be available to analyze this multi-non-linear factors rotor effectively and can reveal the exact fault characteristics in detail.

1. Introduction

In traditional dynamic analysis of rotor system, linear models based on the superposition principle have been proven to be very useful. However, in practice, many systems are non-linear. Especially, with more rapid angular velocity, there are many phenomena that cannot be explained by linear model. To design or analyze real large turbo machinery, such as turbines, generators and aviation engines, more and more non-linear factors have to be taken into account. There are same questions in the filed of faults diagnosis. And recently, the coupling effect of multi-non-linear factors on rotor system is a new focus.

To solve this question, the experts and technologists allover the world apply some advanced techniques, such as computer techniques, updated non-linear dynamic theory, wavelet analysis

*Corresponding author. Tel.: +86-29-3067190; fax: +86-29-2668301.
E-mail address: wan7190@pub.xaonline.com (F. Wan).

0022-460X/03/$ - see front matter © 2003 Elsevier Ltd. All rights reserved.
doi:10.1016/S0022-460X(03)00277-3

techniques and nerve net techniques, etc. These techniques can overcome the disadvantage of traditional methods. Harmonic Wavelet, one of orthogonal wavelets, was developed for practical purpose by Newland [1–3]. Because of the outstanding capacity of time–frequency decomposition and implementation arithmetic is simple and easy harmonic wavelet transform (HWT) is employed in many fields, e.g., investigate the elastic beam vibration [4], to analyze the vibration signal of rotating machines [5] and also to evaluate the dispersive phase and group velocities [6].

In this paper, a Jeffcott rotor sliding bearings system, with rotor–stator rubbing and a small transverse crack on its shaft, is investigated. As Sekhar [7] has proved, the vibration of rotating system will become more severe when its velocity is increasing. When the displacement of the disk center exceeds the clearance of the stator and the rotor, there will be rub-impact. In this case, three non-linear factors (non-linear oil film forces, rotor–stator rubbing and the presence of crack) may affect the dynamic characteristics of the system simultaneously and make it become more complex. Its unstable dynamic response should be calculated with numerical method and analyzed using time–frequency technology. For the purpose of detection and diagnosis of these faults, time–frequency maps of HWT are applied for showing the vibration characteristics in detail.

The presence of crack and rotor–stator rubbing are two general faults in most rotor system and there has been extensive research on them. A comprehensive survey of simple rotors with transverse crack has been presented by Gash [8]. Sekhar has analyzed the transient response of cracked rotor passing through critical speed [9] and investigated the effects of crack depth, unbalance eccentricity with phase and acceleration [7]. Meng [10] has researched the dynamic response in the sub-critical and super-critical speed range and used the cross-coupling stiffness terms to detect crack. George [11] has presented a new method to identify the depth and the location of a transverse surface crack by measuring the coupled response. Mayes [12] analyzed the responses of multi-rotor bearing system when a rotor has a transverse crack.

On the other hand, investigation of the characteristics of rotor–stator rubbing is also extensive. Beaty [13] has calculated the response in terms of a Fourier series expansion and explained the various components of it. The transient response has been analyzed by Choy [14] and the effect of imbalance load and friction has been discussed. Considering the oil film force, Chu [15] has found that a rub-impact rotor system can exhibit very rich forms of motion, e.g., periodic, quasi-periodic and chaotic vibrations.

All these works have helped research on the real rotor systems. But the coupling effect of the crack and the rubbing is the keystone of this paper. HWT is applied to reveal its characteristics in both time and frequency domains.

2. Equation of motion

Fig. 1 shows a simple Jeffcott rotor with transverse crack on its shaft in the inertial co-ordinates $x-y$ and rotating co-ordinates $\zeta-\xi$. The disk is located at the midspan of the shaft and the bearings at both ends are same, sliding ones.

If (x_d, y_d) and (x_b, y_b) represent the co-ordinates of the center of the disk and the journal, respectively. With constant angular velocity ω, the equation of motion of the rotor sliding bearing

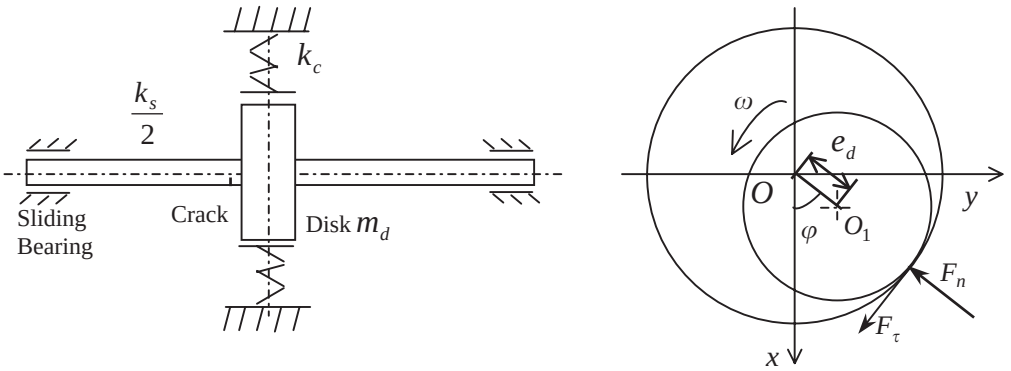

Fig. 1. Analytical model of rotor sliding bearing system and its rubbing force.

system can be written as follows:

$$\begin{aligned}
&m_d\ddot{x}_d + c(\dot{x}_d - \dot{x}_b) + k_x(x_d - x_b) = m_d g + m_d e_p \omega^2 \cos\theta,\\
&m_d\ddot{y}_d + c(\dot{y}_d - \dot{y}_b) + k_y(y_d - y_b) = m_d e_p \omega^2 \sin\theta,\\
&m_b\ddot{x}_b + c(\dot{x}_b - \dot{x}_d)/2 + k_x(x_b - x_d)/2 = m_b g + P_x,\\
&m_b\ddot{y}_b + c(\dot{y}_b - \dot{y}_d)/2 + k_y(y_b - y_d)/2 = P_y,
\end{aligned} \tag{1}$$

where m_d is the mass of the disk, m_b is the mass at the bearings, c is external damping, e_p is eccentricity of the disk, and k_x, k_y are stiffnesses of the cracked shaft in x and y orientations, respectively.

2.1. Crack model

There are several models of the cracked shaft. If a cracked shaft rotates slowly under the load of its own weight, the crack will open and close once a revolution. Its breathing motion can be described by the steering function $f(\theta)$. Hinge model [7–9] and smooth function model [12] can be used. For small cracks, Gash considered the simple hinge model as a good model [8]. The present study assumes the dominance of weight, and the hinge model is adopted:

$$f(\theta) = \begin{cases} 1, & 0 < \theta < \dfrac{\pi}{2}, \dfrac{3\pi}{2} < \theta < 2\pi, \\ 0, & \dfrac{\pi}{2} \leqslant \theta \leqslant \dfrac{3\pi}{2}. \end{cases} \tag{2}$$

Based on the hinge model, the stiffness matrix for the cracked shaft can be derived [7,9]:

$$\begin{Bmatrix} k_x \\ k_y \end{Bmatrix} = k_s - \frac{1}{2} f(\theta) \Delta k_\zeta \begin{bmatrix} 1 + \cos 2\theta & \sin 2\theta \\ \sin 2\theta & 1 - \cos 2\theta \end{bmatrix}, \tag{3}$$

where k_s is the stiffness of the shaft without crack and Δk_ζ is the variation of stiffness in ζ orientation in rotating co-ordinates. The modulus of Δk_ζ is far larger than that of Δk_ξ. The rotating angle satisfies $\theta = \omega t + \beta$ and β is the phase between the eccentricity and the center of the crack, i.e., crack angle.

2.2. Oil film force of the bearing

For a squeeze-film bearing, when it is static, the eccentricity of the center of the journal $e_b = \sqrt{x_b^2 + y_b^2}$, phase $\psi = \text{arctg}(y_b/x_b)$ and $\varepsilon = e_b/c_p$. Its basic lubrication equation governing the oil film is the Reynolds equation can be written in the following form [16]:

$$\frac{1}{R^2}\frac{\partial}{\partial\theta}\left(\frac{h^3}{12\eta}\frac{\partial p}{\partial\theta}\right) + \frac{\partial}{\partial z}\left(\frac{h^3}{12\eta}\frac{\partial p}{\partial z}\right) = \frac{1}{2}(\omega - 2\dot{\psi})\frac{\partial h}{\partial\theta} + \dot{e}_b\cos\theta, \tag{4}$$

where p is the supply pressure of the oil, $h = C(1 + \varepsilon\cos\theta)$ is the oil-film thickness.

Under the assumption of short bearing approximation, the bearing-land length L is far less than the bearing diameter $2R$, and the variation of oil film force in the circumferential orientation $\partial p/\partial\theta$ can be neglected. The Reynolds equation can be rewritten as

$$\frac{\partial}{\partial z}\left(\frac{h^3}{12\eta}\frac{\partial p}{\partial z}\right) = \frac{1}{2}(\omega - 2\dot{\psi})\frac{\partial h}{\partial\theta} + \dot{e}_b\cos\theta, \tag{5}$$

Then the pressure can be obtained by

$$p(\theta, z) = \frac{3\eta}{C^2(1 + \varepsilon\cos\theta)^3}\left(z + \frac{L}{2}\right)\left(z - \frac{L}{2}\right)[-(\omega - 2\dot{\psi})\varepsilon\sin\theta + 2\dot{\varepsilon}\cos\theta]. \tag{6}$$

Radial and circumferential forces P_ε and P_ψ emanating from the squeeze film are obtained by integration of the pressure distribution over the entire journal surface:

$$\begin{aligned} P_\varepsilon &= -\int_{-L/2}^{L/2} \mathrm{d}z \int_0^{2\pi} p(\theta, z)\cos\theta R\,\mathrm{d}\theta, \\ P_\psi &= \int_{-L/2}^{L/2} \mathrm{d}z \int_0^{2\pi} p(\theta, z)\sin\theta R\,\mathrm{d}\theta. \end{aligned} \tag{7}$$

Based on the Sommerfeld condition $p|_{\theta=\pi} = 0$ and the boundary condition $p|_{\theta=0} = 0$, the oil film forces can be obtained:

$$\begin{aligned} P_\varepsilon &= \frac{1}{2}\frac{\eta L R^3}{c_P^2}\left(\frac{L}{R}\right)^2[(\omega - 2\dot{\psi})G_1(\varepsilon) + 2\dot{\varepsilon}G_2(\varepsilon)], \\ P_\psi &= \frac{1}{2}\frac{\eta L R^3}{c_P^2}\left(\frac{L}{R}\right)^2[(\omega - 2\dot{\psi})G_3(\varepsilon) + 2\dot{\varepsilon}G_4(\varepsilon)], \end{aligned} \tag{8}$$

where

$$G_1(\varepsilon) = \frac{2\varepsilon^2}{(1 - \varepsilon^2)^2}, \quad G_2(\varepsilon) = \frac{\pi(1 + 2\varepsilon^2)}{2(1 - \varepsilon^2)^{5/2}}, \quad G_3(\varepsilon) = \frac{\pi\varepsilon}{2(1 - \varepsilon)^{3/2}}, \quad G_4(\varepsilon) = \frac{2\varepsilon}{(1 - \varepsilon^2)^2},$$

Then projecting the oil film force P_ε and P_ψ on the inertial co-ordinates $x - y$, we have

$$\begin{aligned} P_x &= -P_\varepsilon\sin\psi + P_\psi\cos\psi, \\ P_y &= P_\varepsilon\cos\psi + P_\psi\sin\psi. \end{aligned} \tag{9}$$

2.3. Rubbing force

As Sekhar [7,9] has proved the transient vibration responses of Eq. (1) may develop oscillation near the critical speed. With a different parameter, the vibration may be more violent or less severe. If the displacement of center of the disk e_d does not exceed the radial clearance δ between bearing outer race and stator at rest, there is no rubbing and there are no forces. Or else, rubbing happens and the forces may influence the responses. The rubbing forces are the normal force F_n and the frictional force F_τ [13,15]

$$F_n = \begin{cases} 0 & (e_d < \delta), \\ (e_d - \delta)k_c & (e_d \geqslant \delta), \end{cases}$$
$$F_\tau = fF_n, \tag{10}$$

where k_c is radial stiffness of stator and f is coefficient of friction. With $\sin\varphi = y_d/e_d$ and $\cos\varphi = x_d/e_d$, the rubbing force F can be described as follows:

$$\begin{bmatrix} F_x \\ F_y \end{bmatrix} = \begin{bmatrix} 0 \\ 0 \end{bmatrix} \quad (e_d < \delta),$$
$$\begin{bmatrix} F_x \\ F_y \end{bmatrix} = -\frac{k_c(e_d - \delta)}{e_d}\begin{bmatrix} 1 & -f \\ f & 1 \end{bmatrix}\begin{bmatrix} x_d \\ y_d \end{bmatrix} \quad (e_d \geqslant \delta). \tag{11}$$

Therefore, when the rotor system is rubbing, its dynamic equations can be rewritten as

$$m_d\begin{Bmatrix} \ddot{x}_d \\ \ddot{y}_d \end{Bmatrix} + c\begin{Bmatrix} \dot{x}_d - \dot{x}_b \\ \dot{y}_d - \dot{y}_b \end{Bmatrix} + \begin{bmatrix} k_x & 0 \\ 0 & k_y \end{bmatrix}\begin{Bmatrix} x_d - x_b \\ y_d - y_b \end{Bmatrix} = \begin{Bmatrix} F_x \\ F_y \end{Bmatrix} + \begin{Bmatrix} m_d g + m_d e_p \omega^2 \cos\theta \\ m_d e_p \omega^2 \sin\theta \end{Bmatrix},$$
$$m_b\begin{Bmatrix} \ddot{x}_b \\ \ddot{y}_b \end{Bmatrix} + \frac{c}{2}\begin{Bmatrix} \dot{x}_b - \dot{x}_d \\ \dot{y}_b - \dot{y}_d \end{Bmatrix} + \frac{1}{2}\begin{bmatrix} k_x & 0 \\ 0 & k_y \end{bmatrix}\begin{Bmatrix} x_b - x_d \\ y_b - y_d \end{Bmatrix} = \begin{Bmatrix} m_b g \\ 0 \end{Bmatrix} + \begin{Bmatrix} P_x \\ P_y \end{Bmatrix}. \tag{12}$$

Substituting Eqs. (3), (8) and (10) into Eq. (11), the equation of motion of casing rotor–stator rubbing can be written in dimensionless form by dividing both side by $m_d\omega_0^2$:

$$\begin{Bmatrix} x_1'' \\ y_1'' \end{Bmatrix} + 2D\begin{Bmatrix} x_1' - x_2' \\ y_1' - y_2' \end{Bmatrix} + \left(\begin{bmatrix} 1 & 0 \\ 0 & 1 \end{bmatrix} - \frac{f(\theta)\Delta k}{2}\begin{bmatrix} 1+\cos 2\mu\tau & \sin 2\mu\tau \\ \sin 2\mu\tau & 1-\cos 2\mu\tau \end{bmatrix}\right)\begin{Bmatrix} x_1 - x_2 \\ y_1 - y_2 \end{Bmatrix}$$
$$+ \beta\left(1 - \frac{\delta}{e_d}\right)\begin{bmatrix} 1 & -f \\ f & 1 \end{bmatrix}\begin{Bmatrix} x_1 \\ y_1 \end{Bmatrix} = \begin{Bmatrix} W_g \\ 0 \end{Bmatrix} + e_p\mu^2\begin{Bmatrix} \cos(\mu\tau + \varphi_0) \\ \sin(\mu\tau + \varphi_0) \end{Bmatrix},$$

$$\begin{Bmatrix} \alpha x_2'' \\ \alpha y_2'' \end{Bmatrix} + D\begin{Bmatrix} x_2' - x_1' \\ y_2' - y_1' \end{Bmatrix} + \frac{1}{2}\left(\begin{bmatrix} 1 & 0 \\ 0 & 1 \end{bmatrix} - \frac{f(\theta)\Delta k}{2}\begin{bmatrix} 1+\cos 2\mu\tau & \sin 2\mu\tau \\ \sin 2\mu\tau & 1-\cos 2\mu\tau \end{bmatrix}\right)\begin{Bmatrix} x_2 - x_1 \\ y_2 - y_1 \end{Bmatrix}$$
$$= \begin{Bmatrix} \alpha \cdot W_g \\ 0 \end{Bmatrix} + \frac{\pi(1+2\alpha)}{4}\frac{S_0 \cdot W_g}{\sqrt{x_2^2 + y_2^2}}\left(\frac{L}{R}\right)^2\begin{bmatrix} \bar{P}_\psi & -\bar{P}_\varepsilon \\ \bar{P}_\varepsilon & \bar{P}_\psi \end{bmatrix}\begin{Bmatrix} x_2 \\ y_2 \end{Bmatrix}, \tag{13}$$

where $\mu = \omega/\omega_0$ in which $\omega_0 = \sqrt{k_s/m_d}$, $\alpha = m_b/m_d$, $\beta = k_c/k_s$, $\Delta k = \Delta k_\xi/k_s$ (the crack parameter), $D = c/2\omega_0 m_d$, $W_g = g/\omega_0^2$, $W = m_b g + \frac{1}{2} m_d g$ and Sommerfeld number $S_0 = \eta\omega_0 RL/\pi W(R/c_p)^2$ [16].

3. Numerical results and its harmonic wavelet transform

3.1. Harmonic wavelet transform and wavelet maps

Wavelet transform is one of the fundamental correlation methods. The wavelet coefficient $a(t)$, which provides information about the input signal $f(t)$ and its relation to the shape of wavelet function $w(t)$, is defined by the following correlation equation:

$$a(t) = \int_{-\infty}^{\infty} f(\tau) w^*(\tau - t)\, \mathrm{d}\tau, \tag{14}$$

where $w^*(t)$ is the complex conjugate of $w(t)$. If $f(t)$ correlates with $w(t)$, $a(t)$ will be a large value. If they do not correlate, $a(t)$ will be very small. Any waveform can be used for the wavelet if it is localized at a particular time.

Harmonic wavelets are orthogonal wavelets. In the frequency domain, harmonic wavelets are simple structured as

$$W_{m,n}(\omega) = \begin{cases} \dfrac{1}{(n-m)2\pi}, & m2\pi \leqslant \omega \leqslant n2\pi, \\ 0, & \text{elsewhere}, \end{cases} \tag{15}$$

where n and m are real but are not necessarily integers. So the harmonic wavelets can be related to the ideal bandpass filter. Harmonic wavelet functions, $w_{m,n}(t)$, in the time domain can be obtained from the inverse Fourier transform of $W_{m,n}(\omega)$:

$$w_{m,n}(t) = \frac{\mathrm{e}^{\mathrm{j}n2\pi t} - \mathrm{e}^{\mathrm{j}m2\pi t}}{\mathrm{j}(n-m)2\pi t}, \tag{16}$$

where $\mathrm{j} = \sqrt{-1}$. If this wavelet is translated by step $k/(n-m)$, Eq. (16) becomes

$$w_{m,n}\left(t - \frac{k}{n-m}\right) = \frac{\mathrm{e}^{\mathrm{j}n2\pi(t-(k/(n-m)))} - \mathrm{e}^{\mathrm{j}m2\pi(t-(k/(n-m)))}}{\mathrm{j}2\pi(n-m)(t-(k/(n-m)))}, \tag{17}$$

which is the expression for a general harmonic wavelet of bandwidth $2(n-m)\pi$ that is centered at $t = k/(n-m)$.

The wavelet transform allows an arbitrary function $f(t)$ to be expressed as a series expansion, just like the Fourier expansion. For harmonic wavelet described as Eq. (17), the corresponding expansion formula is

$$f(t) = a_0 + \sum_{m,n} \sum_{k=0}^{n-m-1} \left\{ a_{m,n,k} w_{m,n}\left(x - \frac{k}{n-m}\right) + a^*_{m,n,k} w^*_{m,n}\left(x - \frac{k}{n-m}\right) \right\}, \tag{18}$$

where $a_{m,n,k}$ and $a^*_{m,n,k}$ are the complex harmonic wavelet coefficients and are defined by

$$a_{m,n,k} = (n-m)\int_{-\infty}^{\infty} f(\tau) w^*_{m,n}\left(\tau - \frac{k}{n-m}\right) \mathrm{d}\tau,$$

$$a^*_{m,n,k} = (n-m)\int_{-\infty}^{\infty} f(\tau) w_{m,n}\left(\tau - \frac{k}{n-m}\right) \mathrm{d}\tau. \tag{19}$$

If the real function f_r, i.e., the discrete series of $f(t)$ with $r = 0$ to $N-1$ ($N = 2^n$), is analyzed by the DFT into its harmonics, then according to Parseval's theorem

$$\frac{1}{N}\sum_{r=0}^{N-1} f_r^2 = \sum_{i=0}^{n-1} |F_i|^2. \tag{20}$$

For harmonic wavelets of bandwidth $m2\pi \leqslant \omega \leqslant n2\pi$, the corresponding expansion equation is

$$\frac{1}{N}\sum_{r=0}^{N-1} f_r^2 = a_0^2 + \sum_{m,n}\frac{2}{n-m}\sum_{k=0}^{n-m-1} |a_{m,n,k}|^2 + a_{N/2}^2. \tag{21}$$

If the bandwidth increases in octaves, Eq. (21) becomes

$$\frac{1}{N}\sum_{r=0}^{N-1} f_r^2 = a_0^2 + \sum_{i=0}^{n-2}\frac{1}{2^{i-1}}\sum_{k=0}^{2^i-1} |a_{2^i+k}|^2 + a_{N/2}^2. \tag{22}$$

Based on this equation, the harmonic wavelet coefficients can be calculated by FFT and IFFT as Newland [2,3] had expressed. For a real input sequence of length $2^4 = 16$, the implementation procedure can be illuminated as Fig. 2. And the wavelet map, which is obtained by plotting the magnitude of the wavelet coefficients with time and frequency, is usually adapted to describe the characteristics of transient oscillation signal. Newland used grid base (as Fig. 3) to explain the harmonic wavelet maps. There are $n+1$ wavelet levels running from -1 to $n-1$, and 2^{n-2} position steps. At level -1, all the heights are set equal to a_0^2; at level $i \leqslant (n-1)$, there are 2^i positions and two amplitudes are located at each position. The two terms are complex conjugates. Therefore, the sum of these two terms is equal to two times the first term (Fig. 3): $|a_{2^i+k}|^2 + |a_{2^n-2^i-k}|^2 = 2|a_{2^i+k}|^2$, where $k = 0 \sim 2^i - 1$. More wavelet levels, equivalent to greater frequency discrimination on the y-axis, means fewer position steps, which gives less precision of position on the x-axis.

3.2. Vibration analysis by HWT

The transient vibration response of Eq. (13) is always unstable. As described above, the harmonic time–frequency maps can reveal its characteristics in detail. With the following data of the rotor-system, $D = 0.12$, $f = 0.025$, $\Delta k = 0.35$, $\beta = 3$, $e_p = 0.1$ mm, $\delta = 0.1$ mm, $\varphi_0 = 0$, $\alpha = 0.10$, $S_0 = 0.06$, and assuming the initial value is $x = y = 0.001$ and $v_x = v_y = 0.0$, the transient response can be calculated using Newmark method and analyzed by HWT.

Fig. 4 shows the frequency spectra, time–frequency mesh maps and time–frequency contour maps of the system. From its frequency spectra, many frequency components can be found. In this paper, wavelet maps include two kinds, time–frequency mesh maps and time–frequency counter maps. They are always used together to show the characteristics of signals. Time–frequency contour maps are projections of time–frequency mesh maps. And levels on the y-axis

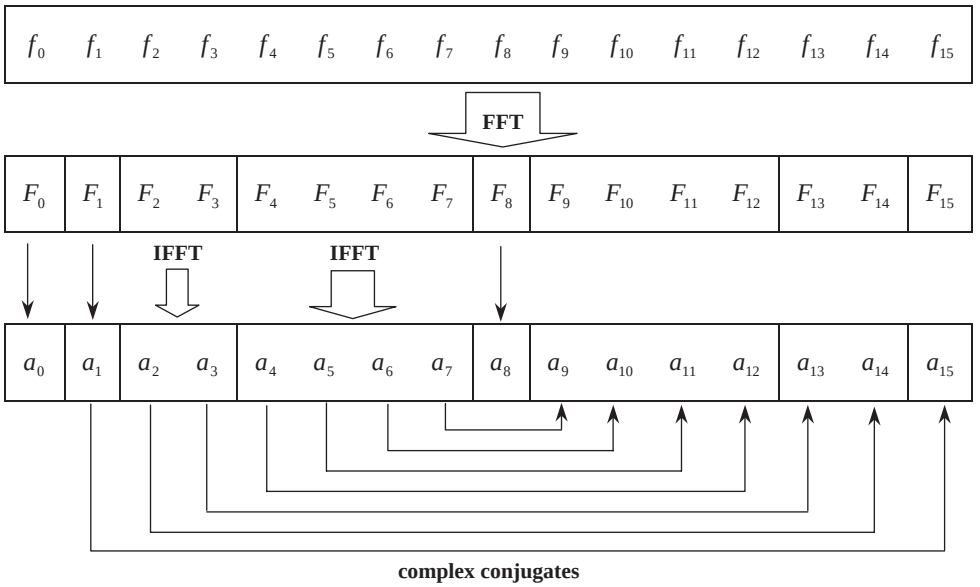

Fig. 2. Implementation procedures of HWT for a real input f_r, $r = 0 - 15$.

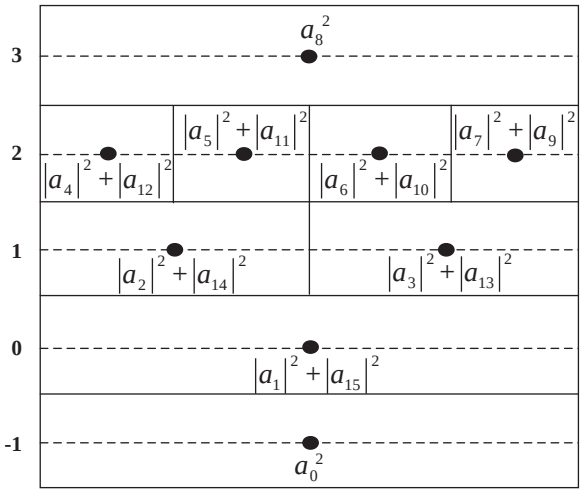

Fig. 3. Grid base for plotting a harmonic wavelet map of f_r, $r = 0 - 15$.

are related to frequency, positions on x-axis are related to time. Ridges of mesh maps are the square of wavelet coefficients. Then wavelet maps will show the signals in time and frequency domain simultaneously. In x orientation, the maximal peak appears between 128 and 256 positions. During 512–640 positions and 768–896 positions, there are other peaks too. In y orientation, the responses are stable between 512 and 640 positions, so its contour is zero. During positions 128–256, 384–512 and 768–896, its contours are dense, and their corresponding maps appear as peaks. According to Fig. 4, especially, during positions 384–640 and 896–1024 the contour maps are entirely different in both orientations.

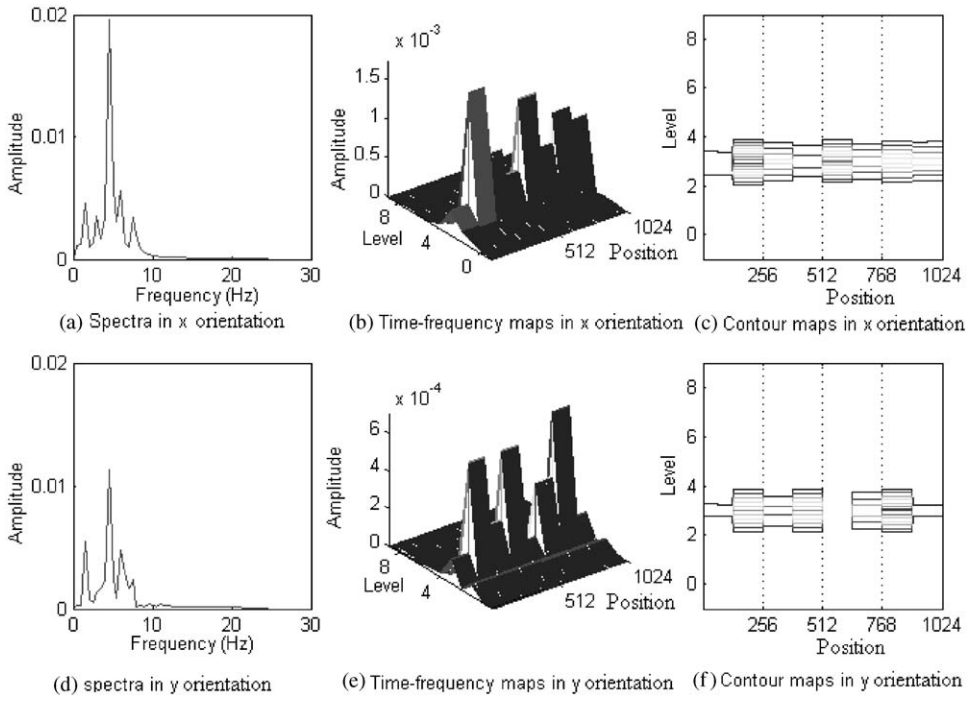

Fig. 4. Spectra, time–frequency mesh maps and contour maps of cracked rotor sliding bearing system casing rubbing.

Without considering the bearing oil film force and keeping other parameters invariable, the frequency spectra, time–frequency mesh maps and time–frequency contours of the system are showed by Fig. 5. Comparing Fig. 5 with Fig. 4, it can be easily found that differences are obvious. Without oil film force, its responses in x orientation are located on the 4th wavelet decomposition level. Its contours keep almost the same density in all positions. Its time–frequency mesh maps almost have the same peak too. But in y orientation, its contours do not centralize at one level but spread from 2 to 5 levels. The variety of the ridges is not so remarkable as in Fig. 4(e). According to this, the effect of oil film force on the rotor system is tremendous. To investigate a real rotor system, the force from the bearing oil film must be considered.

As explained above, if the displacement of center of the disk e_d does not exceed the radial clearance δ between bearing outer race and stator at rest, there is no rubbing and there are no forces. In this case, the corresponding wavelet maps are presented as Fig. 6. In comparison with Fig. 4(a), the high frequency components of its spectra disappear. During positions 1–128 its x orientation contours and time–frequency mesh maps become more complex. After 128 positions, its contours are almost of the same density and its peaks of time–frequency maps vary unremarkably. But the contours decentralize from 2 to 4 levels. In y orientation, there are no zero contours. And its contours are similar as in x orientation. Based on comparison of Fig. 6 with Fig. 4, the effect of the rub-impact force on the rotor system can be explained clearly. Whether the possibility of rub-impact is considered or not, the rotor system may exhibit different dynamic characteristics. This requires us to pay attention to this question.

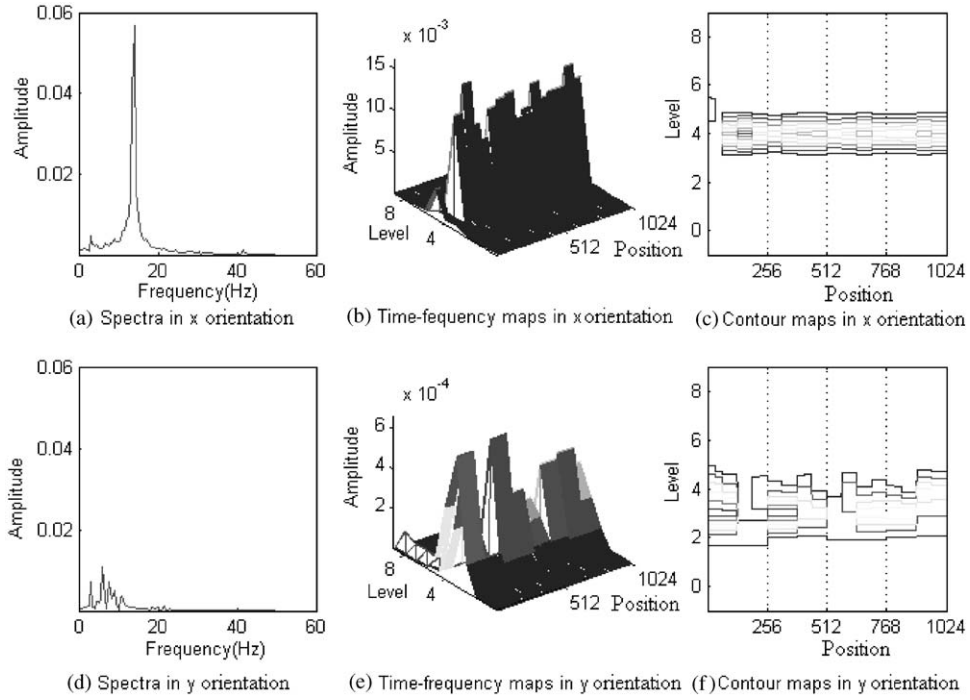

Fig. 5. Spectra, time–frequency mesh maps and contour maps of cracked rotor system casing rubbing and no oil film force.

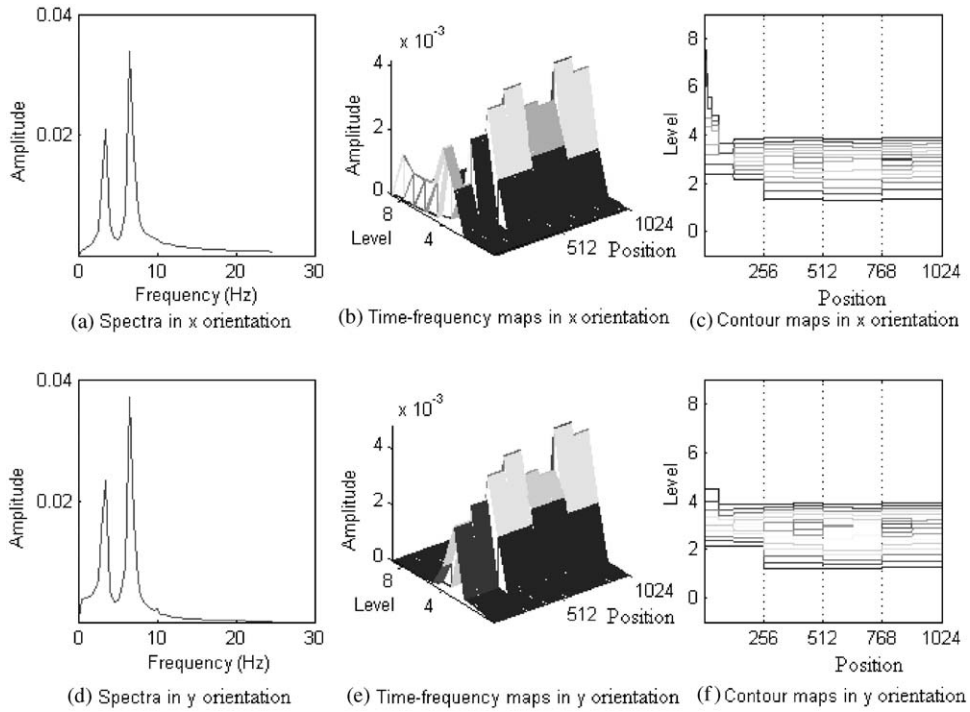

Fig. 6. Spectra, time–frequency mesh maps and contour maps of cracked rotor sliding bearing system casing no rubbing.

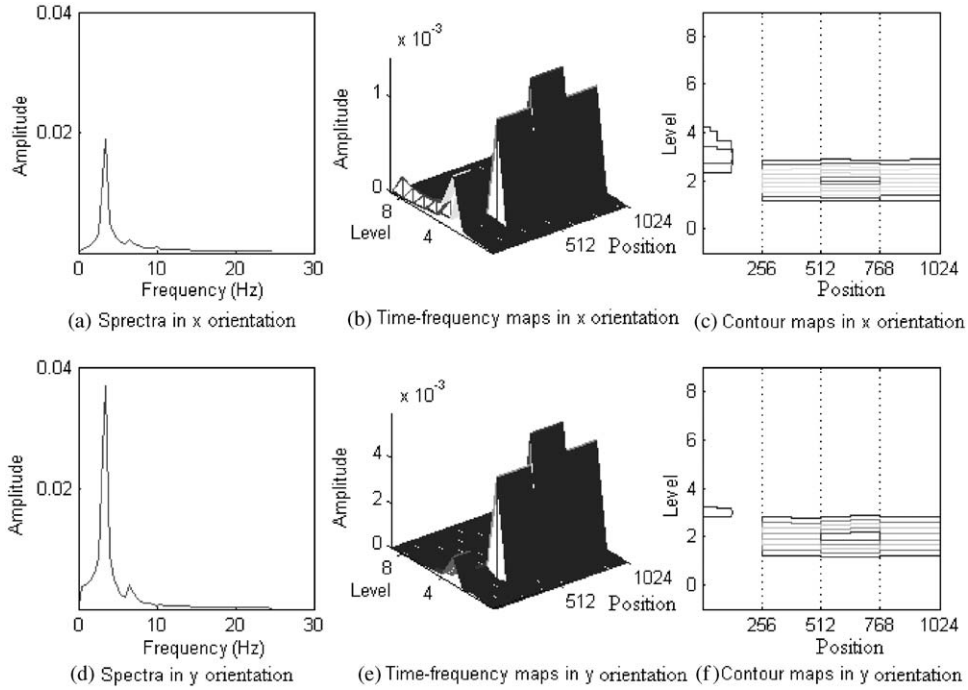

Fig. 7. Spectra, time–frequency mesh maps and contour maps of non-cracked rotor sliding bearing system casing rubbing.

In Eq. (13), if $\Delta k = 0$, the effect of crack is zero. There are only two non-linear factors in this system, oil film force and rub-impact force. The rotor system becomes a rotor supported by oil film bearings and rotor-to-stator rubbing occurs. In this case, its spectra and analysis results by HWT are illustrated in Fig. 7. There are zero contours in both x and y orientations during positions 128–256. After 256 position, its ridges are almost invariable in both orientations. Between positions 1 and 128 there are sparse contours and corresponding peaks are there in time–frequency mesh maps. Comparing with Fig. 4, its dynamic characteristics in this case are completely different. These great peaks in Fig. 4 all disappear, and the positions of these zero contours are also different. These tell us that the effects of rub-impact force and the crack are coupled and should not be investigated.

4. Conclusion

From the analysis, several conclusions can be drawn. Firstly, HWT may be a feasible and efficient technique to analyze a multi-non-linear factors rotor. The time–frequency mesh maps and contours can reveal the dynamic characteristics of the rotor system in detail. They can reveal many complex characteristics that cannot be discovered by FFT spectra. Secondly, the effect of the bearings oil film force on system is significant and should be considered adequately. In sliding rotor, the oil film forces always exist. To analyze and diagnose this rotor system, the supporting

bearings and its forces must be considered. Thirdly, the effect of multi-non-linear factors is coupling and must be considered simultaneously. It is necessary to consider each vital factor and set up a reasonable non-linear dynamic model. Then, detection and diagnosis of rotor bearing system can be performed accurately.

Acknowledgements

The authors would like to acknowledge the support of National Science Foundation through No. 50275113.

References

[1] D.E. Newland, Harmonic wavelet analysis, Proceedings of the Royal Society of London Series A 443 (1993) 203–225.
[2] D.E. Newland, Wavelet analysis of vibration, Part 1: theory, Transactions of the American Society of Mechanical Engineers, Journal of Vibration and Acoustics 116 (1994) 409–416.
[3] D.E. Newland, Wavelet analysis of vibration, Part 2: wavelet maps, Transactions of the American Society of Mechanical Engineers, Journal of Vibration and Acoustics 116 (1994) 417–425.
[4] D.E. Newland, Ridge and phase identification in the frequency analysis of transient signals by harmonic wavelets, Transactions of the American Society of Mechanical Engineers, Journal of Vibration and Acoustics 121 (1999) 149–155.
[5] S.M. Li, Q.Y. Xu, The fractal analysis about rotor vibration signal of high-speed air compressor, Proceedings of the Third International Symposium on Test and Measurement (ISTM99), 1999, pp. 717–720.
[6] H.C. Park, D.-S. Kim, Evaluation of the dispersive phase and group velocities using harmonic wavelet transform, NTD&E International 34 (2001) 457–467.
[7] A.S. Sekhar, B.S. Prabhu, Condition monitoring of cracked rotors through transient response, Mechanism and Machine Theory 33 (1998) 1167–1175.
[8] R. Gash, A survey of the dynamic behavior of a simple rotating shaft with a transverse crack, Journal of Sound and Vibration 160 (1993) 313–332.
[9] A.S. Sekhar, B.S. Prabhu, Transient analysis of a cracked rotor passing through critical speed, Journal of Sound and Vibration 173 (1994) 415–421.
[10] M. Guang, The nonlinear influences of whirl speed on the stability and response of a cracked rotor, Journal of Machine Vibration 6 (1992) 216–230.
[11] G.D. Gounaris, C.A. Papadopoulos, Crack identification in rotating shafts by coupled response measurements, Engineering Fracture Mechanics 69 (2002) 339–352.
[12] I.W. Mayes, W.G.R. Davies, Analysis of the responses of multi-rotor-bearing system containing a transverse crack in a rotor, Transactions of the American Society of Mechanical Engineers, Journal of Vibration, Acoustics, Stress, Reliability in Design 106 (1984) 139–145.
[13] R.F. Beaty, Differentiating rotor response due to radial rubbing, Transactions of the American Society of Mechanical Engineers, Journal of Vibration, Acoustics, Stress, Reliability in Design 107 (1985) 151–160.
[14] F.K. Choy, J. Padovan, Non-linear transient analysis of rotor-casing rub events, Journal of Sound and Vibration 113 (1987) 529–545.
[15] F. Chu, Z. Zhang, Periodic, quasi-periodic and chaotic vibrations of a rub-impact rotor system supported on oil film bearings, International Journal of Engineering Science 35 (1997) 963–973.
[16] Y.E. Zhong, ZH.Y. He, ZH. Wang, et al., Rotor dynamic (In Chinese). Tsinghua University Press, Beijing, 1987.